ADCT-602, a Novel PBD Dimer–containing Antibody–Drug Conjugate for Treating CD22-positive Hematologic Malignancies

Francesca Zammarchi[1], Karin E. Havenith[1], Nikoleta Sachini[1], Narinder Janghra[1], Simon Chivers[1], Esohe Idusogie[2], Eugenio Gaudio[3], Chiara Tarantelli[3], Francois Bertelli[4], Kathleen Santos[4], Peter Tyrer[4], Simon Corbett[5], Filippo Spriano[3], Gaetanina Golino[3], Luciano Cascione[3], Francesco Bertoni[3,6], John A. Hartley[5], and Patrick H. van Berkel[1]

ABSTRACT

Relapsed or refractory B-cell acute lymphoblastic leukemia (R/R B-ALL) and lymphomas have poor patient outcomes; novel therapies are needed. CD22 is an attractive target for antibody–drug conjugates (ADCs), being highly expressed in R/R B-ALL with rapid internalization kinetics. ADCT-602 is a novel CD22-targeting ADC, consisting of humanized mAb hLL2-C220, site specifically conjugated to the pyrrolobenzodiazepine dimer–based payload tesirine. In preclinical studies, ADCT-602 demonstrated potent, specific cytotoxicity in CD22-positive lymphomas and leukemias. ADCT-602 was specifically bound, internalized, and trafficked to lysosomes in CD22-positive tumor cells; after cytotoxin release, DNA interstrand crosslink formation persisted for 48 hours. In the presence of CD22-positive tumor cells, ADCT-602 caused bystander killing of CD22-negative tumor cells. A single ADCT-602 dose led to potent, dose-dependent, *in vivo* antitumor activity in subcutaneous and disseminated human lymphoma/leukemia models. Pharmacokinetic analyses (rat and cynomolgus monkey) showed excellent stability and tolerability of ADCT-602. Cynomolgus monkey B cells were efficiently depleted from circulation after one dose. Gene signature association analysis revealed *IRAK1* as a potential marker for ADCT-602 resistance. Combining ADCT-602 + pacritinib was beneficial in ADCT-602–resistant cells. Chidamide increased CD22 expression on B-cell tumor surfaces, increasing ADCT-602 activity. These data support clinical testing of ADCT-602 in R/R B-ALL (NCT03698552) and CD22-positive hematologic cancers.

Introduction

CD22 is a cell-surface type I transmembrane sialoglycoprotein consisting of 7 extracellular immunoglobulin (Ig) domains and a 141–amino acid cytoplasmic tail (1). It is expressed on the surface of all stages of B-cell development, reaching peak levels on mature B cells. However, its expression is lost upon terminal differentiation to plasma cells (2). CD22 is not expressed on hematopoietic stem cells or other nonlymphoid hematopoietic or nonhematopoietic cells (3). This specific expression profile during B-cell development has made CD22 an attractive molecule for targeted B-cell malignancy therapies.

CD22 expression has been reported in follicular lymphoma, marginal zone lymphoma, mantle cell lymphoma (MCL), diffuse large B-cell lymphoma (DLBCL), small lymphocytic lymphoma, hairy cell leukemia, and chronic lymphocytic leukemia (4, 5). In addition, CD22 is almost universally expressed in B-cell acute lymphoblastic leukemia (B-ALL), including in the relapsed or refractory (R/R) setting (6–8). Various therapeutic modalities against CD22 have been developed, including naked or radiolabeled antibodies (9–11), bispecific antibodies (12, 13), and chimeric antigen receptor T-cell therapy (14, 15). CD22 is known to recycle and partially accumulates in the lysosome (16). Together with the rapid internalization kinetics of CD22 (17), this makes CD22 an attractive target for an immunotoxin or antibody–drug conjugate (ADC) approach, and multiple compounds have been approved (18, 19).

In the CD22-targeting ADC field, although the development of the auristatin-based ADC pinatuzumab vedotin was discontinued for the treatment of non-Hodgkin lymphoma after phase II (20), the calicheamicin-based ADC inotuzumab ozogamicin (21) was approved in 2017 for the treatment of adult patients with R/R B-ALL. Approval was based on the superiority of inotuzumab ozogamicin compared with standard-of-care regimens (complete response: 80.7% vs. 29.4%, $P < 0.001$; undetectable minimal residual disease: 78.4% vs. 28.1%, $P < 0.001$; ref. 22). However, its specific safety profile, which includes veno-occlusive disease (22), remains an ongoing area of concern. Veno-occlusive disease may be attributed to the toxin calicheamicin, which is also used in the CD33-specific ADC gemtuzumab ozogamicin (23). We hypothesized that a CD22-targeted ADC based on a pyrrolobenzodiazepine (PBD) dimer could be active in patients with B-ALL or non-Hodgkin lymphoma while mitigating some of the toxicity issues seen with inotuzumab ozogamicin.

Here, we report the preclinical evaluation of ADCT-602, a novel CD22-targeted ADC based on the PBD dimer payload tesirine

[1]ADC Therapeutics (UK) Ltd, London, United Kingdom. [2]ADC Therapeutics America, Inc, Murray Hill, United States. [3]Institute of Oncology Research, Faculty of Biomedical Sciences, USI, Bellinzona, Switzerland. [4]AstraZeneca (MedImmune/Spirogen), London, United Kingdom. [5]University College London, London, United Kingdom. [6]Oncology Institute of Southern Switzerland, Ente Ospedaliero Cantonale, Bellinzona, Switzerland.

Corresponding Author: Patrick H. van Berkel, ADC Therapeutics (UK) Ltd, 8th Floor, Translation and Innovation Hub Building, Imperial College White City Campus, 84 Wood Lane, London W12 0BZ, United Kingdom. E-mail: Patrick.vanBerkel@adctherapeutics.com

Mol Cancer Ther 2024;XX:XX–XX

doi: 10.1158/1535-7163.MCT-23-0506

This open access article is distributed under the Creative Commons Attribution-NonCommercial-NoDerivatives 4.0 International (CC BY-NC-ND 4.0) license.

©2024 The Authors; Published by the American Association for Cancer Research

(SG3249), site specifically conjugated to hLL2-C220, an engineered version of the hLL2 antibody.

Materials and Methods

Ethical statement

All animal studies complied with the recommendations of the Guide for Care and Use of Laboratory Animals (24) with respect to restraint, husbandry, surgical procedures, feed and fluid regulation, and veterinary care and were performed in facilities that are accredited by the Association for Assessment and Accreditation of Laboratory Animal Care, which assures compliance with accepted standards for the care and use of laboratory animals. The pharmacokinetic studies were conducted in accordance with the requirements of the Animals (Scientific Procedures) Act 1986.

Purification of hLL2-C220 and conjugation of hLL2-C220 to SG3249

hLL2 is a clinically validated, humanized mAb of the IgG1 kappa isotype specific for human CD22, which was derived from the murine antibody LL2 (17). hLL2-C220, the antibody component of ADCT-602, was generated by the introduction of the mutations C219S in the light chain and C225V and C228V in the heavy-chain hinges of the parental hLL2 antibody (Supplementary Fig. S1A). This approach is similar to that previously described for MEDI3726, a prostate-specific membrane antigen, PBD-based ADC with good efficacy and tolerability (25). hLL2-C220 was transiently expressed in Chinese hamster ovary cells and purified by routine protein A purification. hLL2-C220 was conjugated to SG3249, as previously published (25). ADCT-602 was generated via site-specific conjugation of the PBD dimer payload SG3249 to the cysteine at position 219 (C220 according to EU numbering) of each heavy chain (Supplementary Fig. S1B). The ADC was formulated in 30 mmol/L histidine, 200 mmol/L sorbitol, and 0.02% Tween 20, with a pH of 6.0. The solution was filtered (0.22 μm) and stored at −70°C.

Analytic characterization

Characterization of ADCT-602 was performed by size-exclusion chromatography and reduced reverse-phase liquid chromatography, as previously published (26). For peptide mapping, ADCT-602 was denatured with guanidine-HCl, reduced with dithiothreitol (DTT), and alkylated with iodoacetamide. The reduced samples were digested with sequencing-grade trypsin, and the peptides were separated by reverse-phase using ultra-performance liquid chromatography while monitored using an ultraviolet detector at 214 nm and mass spectrometry (MS). The peptides were subsequently identified by their mass (corresponding to the amino acid composition and any potential modifications) and confirmed using MS/MS fragmentation spectra measured using high-resolution MS. The drug-to-antibody ratio (DAR) was calculated from the reverse-phase high-performance liquid chromatography (RP-HPLC) profile as previously described (26).

Human cell lines

Lymphoma cell lines were cultured according to the recommended conditions (Supplementary Table S1). All media were supplemented with FBS (10% or 20%) and penicillin–streptomycin–neomycin (∼5,000 U penicillin, 5 mg streptomycin, and 10 mg neomycin/mL; Sigma). Cell line identity was confirmed before initial screening and at regular intervals thereafter by short tandem repeat DNA fingerprinting using the Promega GenePrint 10 System kit (B9510). Cells were tested before initial screening and periodically thereafter for *Mycoplasma* negativity using the MycoAlert Mycoplasma Detection Kit (Lonza). Cell lines were used for a maximum of two months after thawing (no more than 12–16 passages).

CD22 cell surface density

CD22 cell surface density was determined using Bangs Laboratory's Quantum Simply Cellular Antihuman immunoglobulin G (IgG) beads, per the manufacturer's instructions.

Internalization assay

Ramos cells were exposed to ADCT-602 or B12-C220-SG3249 (1 hour at 4°C) and then incubated at 37°C where appropriate. Following the permeabilization of cells using Tween 20 (0.1% volume-to-volume ratio in PBS) for 15 minutes, samples were washed with the PBS, and centrifuged at 4,000 rpm (4°C). Removal of the supernatant was followed by the addition of a rabbit mAb LAMP-1 (1:400; Cell Signaling Technology) for 1 hour on ice. A further washing step was followed by adding both Alexa Fluor 488 goat anti-human (1:200; Thermo Fisher Scientific) for detecting the ADC and Alexa Fluor 568 goat anti-rabbit (1:200; Thermo Fisher Scientific). Both secondary antibody incubations were performed on ice for 1 hour. Nuclei were counterstained with Hoechst 33342 (Thermo Fisher Scientific), and then the cytospins of cell samples were prepared. The samples mounted in ProLong Gold Antifade (Life Technologies) and cover-slipped.

In vitro cell killing and bystander assay

In vitro cytotoxic activity of ADCT-602, the isotype-control ADC, and SG3199 were assessed in a panel of lymphoma and leukemia cell lines, as previously published (27). Cell viability was measured after 96 hours with the CellTiter 96 AQueous One Solution Cell Proliferation Assay (MTS; Promega) for the panel of 12 lymphoma and leukemia cell lines. MTT (3-[4,5-dimethylthiazol-2-yl]-2,5-diphenyltetrazolium bromide; Sigma-Aldrich) was used for the panel of 57 lymphoma cell lines.

For the bystander assay, Ramos cells were incubated with ADCT-602 for the indicated time points. The conditioned medium was transferred to KARPAS-299 cells and incubated for 4 days, and cell viability was measured with MTS assay.

Assessment of ADCT-602 efficacy in *in vivo* models

Ramos (Burkitt lymphoma), WSU-DLCL2 (DLBCL, germinal center B-cell type), and KARPAS-299 (T-cell lymphoma, anaplastic large cell lymphoma subtype) xenografts were established in 8- to 10-week-old female Fox Chase mice with severe combined immunodeficiency (Charles River Laboratories) by implanting 10^7 cells subcutaneously into their flanks. When group mean tumor volumes reached ∼116 to 132 mm^3, mice were randomly allocated into groups to receive the test agent or vehicle. Each animal was euthanized when its tumor reached the endpoint volume or at the study end. The time to endpoint (TTE) for analysis was calculated for each mouse by the following equation:

$$\text{TTE (days)} = \left(\log_{10}[\text{endpoint volume} - \text{intercept}*]/\text{slope}*\right)$$

where $*$ indicates the slope of the line obtained by linear regression of a log-transformed tumor growth data set.

The log-rank test was used to analyze the significance of differences in TTE between the two groups. For the disseminated xenografts model, 10^7 REH (acute lymphocytic leukemia) cells were inoculated intravenously into 5- to 8-week-old female NOG

mice (Taconic Biosciences). Test compounds were administered intravenously 4 days after tumor cell inoculation. Individual mice were euthanized, and an autopsy was performed when hind leg paralysis (a sign of leukemia development) occurred and/or the body weight decreased by ≥20%. The study was terminated on day 62. The log-rank test was used to determine the significance of the differences in overall survival.

DNA interstrand crosslink determination

Quantification of *in vitro* DNA interstrand crosslinks (ICL) was performed using the single-cell gel electrophoresis (Comet) assay (28) following the protocol and reagents published previously (26).

Pharmacokinetic assays

Male Crl:CD (Sprague-Dawley) rats (Charles River Laboratories; RRID: RGD_734476) were dosed IV with ADCT-602. Blood was collected from tail veins at specified time points; serum was isolated and stored at −80°C. Male and female purpose-bred cynomolgus monkeys (*Macaca fascicularis*) were dosed intravenously with ADCT-602. Blood was collected from the femoral vein/artery at specific time points; serum was isolated and stored at −80°C. In rat and monkey serum, quantification of total antibody and ADC [drug-to-antibody ratio (DAR) >1] were determined using an optimized electrochemiluminescence immunoassay (ECLIA). Calibration curves, quality controls, and study samples were diluted and added to an extracellular recombinant human CD22 directly coated to a Meso Scale Discovery (MSD) plate, to a biotinylated anti-Fc CaptureSelect (Thermo Fisher Scientific) coated to a streptavidin-coated MSD plate, or to a biotinylated anti-PBD antibody coated to a streptavidin plate. The plates were then incubated and washed, and a sulfo-tag–labeled anti-Fc detector antibody (Sanquin Reagents B.V.) was used for measuring the total extracellular CD22-binding antibody, total antibody, or ADC (DAR ≥1). For all assays, the read buffer (MSD) was added, and the plates were read on the MSD QuickPlex Plate Reader (MSD Sector Imager 6000). The determination of free SG3199 in cynomolgus monkey serum was performed, as previously published (27). The pharmacokinetic analysis was performed using Phoenix WinNonlin, version 6.2 (Certara; RRID: SCR_024504), with noncompartmental analysis.

Gene expression signature association analysis

An exploratory analysis was conducted to define differentially expressed transcripts between groups of cell lines based on sensitivity to ADCT-602 using previously reported gene expression profiles obtained with the Illumina HT-12 microarray and with the HTG EdgeSeq Oncology Biomarker Panel (GSE94669; ref. 29), using *limma* (30) with a cutoff of $P < 0.05$. A gene-set enrichment analysis was performed using a ranked list of genes, which were based on the *limma*-defined log fold change, and enriched gene sets were considered in the presence of a false discovery rate <0.05.

ADCT-602 and pacritinib combination studies

ADCT-602 was dissolved in water at a concentration of 32 μmol/L, while pacritinib was dissolved in dimethyl sulfoxide (DMSO) at a concentration of 10 mmol/L, according to the manufacturer's instructions. The combination of ADCT-602 and pacritinib was assessed in eight lymphoma cell lines [four high IRAK1 expression levels resistant to ADCT-602 (KARPAS-422, REC1, SU-DHL-16, and TOLEDO) and four low IRAK1 expression levels sensitive to ADCT-602 (FARAGE, OCI-LY-1, VAL, and SP49); Supplementary Table S1]. Synergism assessment was performed by exposing cells (96 hours) to ADCT-602 (6.4 pmol/L–100 nmol/L; 1- to 5-fold dilution) and pacritinib (27.4 nmol/L–20 μmol/L; 1- to 3-fold dilution) alone or in combination, followed by MTT assay. Chou–Talalay combination index (CI) values were determined, as published previously (29). Median CIs were obtained by exposing cell lines to eight increasing concentrations of each compound, either alone or in combination. Concentrations that resulted in ≤10% of the proliferation observed with the single agent were excluded from the CI calculation. Combinations were defined as synergistic (median CI, <0.9), additive (median CI, 0.9–1.1), or of no benefit/antagonist (median CI, >1.1).

Combination studies with chidamide

Chidamide (Selleckchem) was dissolved in DMSO according to the manufacturer's instructions. Cells were treated with chidamide (0.25 or 0.5 μmol/L) for 7 days at 37°C in a 5% carbon dioxide, humidified incubator. On day 3, cells were centrifuged, and fresh medium containing the corresponding concentrations of chidamide was added. The control group was treated with equal volumes of DMSO.

CD22 cell-surface expression after chidamide treatment was measured by flow cytometry. hLL2-C220 and B12 antibodies, followed by Alexa Fluor 488 antihuman secondary antibodies (Thermo Fisher Scientific, catalog no. H10120; RRID: AB_2536548) or allophycocyanin antihuman secondary antibodies (BioLegend, catalog no. 409306, RRID: AB_11150590), were used for CD22 detection. Cells were analyzed using a CytoFLEX Flow Cytometer (Beckman Coulter), and data were analyzed with FlowJo software version 10.8.1 (BD Biosciences; RRID: SCR_008520).

After treatment with chidamide or DMSO, cells were incubated with serial dilutions of ADCT-602 or the nonbinding control ADC for 5 days. Cell viability was measured with the CellTiter 96 AQueous One Solution Cell Proliferation Assay (Promega). Data were normalized to untreated control cells. The 50% inhibitory concentration (IC_{50}) values were determined using GraphPad software (GraphPad; RRID: SCR_002798). The mean and SEs of three independent IC_{50} values were determined.

Data availability statement

The data generated in this study are available upon request from the corresponding author.

Results

Characterization of ADCT-602

Analysis of ADCT-602 by size-exclusion chromatography showed that it was 98% monomeric (Supplementary Fig. S1C), while the DAR was determined to be ∼1.52 (Supplementary Fig. S1D). This DAR was consistently lower compared with the theoretical DAR of 2, which was previously described for MEDI3726 (25) and was likely due to conformational constraints in the antigen-binding fragments of the antibody. However, given the site-specific nature of this approach and the fact that this approach would not result in any higher DAR species that are potentially more toxic, we decided to pursue this format. An in-depth analysis of ADCT-602 by LC/MS peptide mapping confirmed the full sequences of the heavy and light chains of hLL2-C220 (99% heavy chain and 100% light chain), including the N and C termini, and the mutations introduced in either chain [C219S in the light chain (peptide LC:T20–21) as well as C225V and C228V in the heavy chain (peptide HC:T19) and the site-specific conjugation of SG3249 on Cys219 in the heavy chain of hLL2-C220 (peptide HC:T18&)]. No SG3249 was detected on any other fragment (Supplementary Fig. S1E; Supplementary Table S2).

In vitro cytotoxicity of ADCT-602 in lymphoma and leukemia cell lines

ADCT-602 selectively inhibited the growth of a panel of 9 CD22-positive cancer cell lines derived from human lymphomas and leukemias (Daudi, NAMALWA, Ramos, DO HH-2, GRANTA-519, MEC-2, NALM-6, REH, and SEM), while no differential cytotoxicity with an isotype control ADC (B12-C220-SG3249) was observed in three CD22-negative cell lines (KM-H2, SUP-T1, and KARPAS-299; **Table 1**). The PBD dimer cytotoxin SG3199 alone displayed potent cytotoxicity in all 12 cancer cell lines, independent of CD22 expression. No correlation was observed between CD22 expression and either ADCT-602 or SG3199 cytotoxicity, with Pearson correlation coefficients (r) of -0.47 ($P = 0.12$) and -0.037 ($P = 0.91$), respectively.

The *in vitro* cytotoxic activity of ADCT-602 was tested in a larger panel of lymphoma cell lines ($n = 57$; incubation time, 96 hours) (Supplementary Table S3), including both B- and T-cell–derived human lines (48 and 9 cell lines, respectively); individual IC_{50} values for each of the 57 cell lines are shown in Supplementary Table S3. ADCT-602 was more active in B-cell (median IC_{50} 200 pmol/L) than in T-cell (median IC_{50} 1,850 pmol/L) lymphomas (Student t test, $P < 0.005$; Supplementary Table S3; Supplementary File S1), in line with CD22 expression patterns (Supplementary Table S4). The cytotoxic activity of ADCT-602 was similar in models derived from germinal center B-cell–like DLBCL, activated B-cell–like DLBCL, MCL, marginal zone lymphoma, chronic lymphocytic leukemia, and primary mediastinal B-cell lymphoma but was lower in Hodgkin lymphoma (Supplementary Table S3). Among the B-cell lymphoma cell lines, the *in vitro* activity of ADCT-602 did not correlate with CD22 expression measured as cell-surface protein levels (absolute quantitation, $n = 45$, $r = -0.238$, and $P = 0.1$; Supplementary Fig. S2A) or RNA levels using either Illumina HT-12 microarrays ($n = 42$, $r = -0.28$, and $P = 0.07$; Supplementary Fig. S2B) or the HTG EdgeSeq Oncology Biomarker Panel ($n = 36$, $r = -0.24$, and $P = 0.16$; Supplementary Fig. S2C).

The mode of action of ADCT-602

CD22-expressing Ramos cells treated with ADCT-602 showed prominent cell-surface binding (0 hours; **Fig. 1A**). On incubation at 37°C, ADCT-602 showed cellular internalization and colocalization of ADCT-602 with lysosomal-associated membrane protein 1 (LAMP-1) at both 1- and 2-hour time points (**Fig. 1A**) with some intracellular ADC visible at 4 hours. There was no residual ADC staining at 24 hours, suggesting complete lysosomal degradation. In contrast, there was no evidence of membrane binding on the treatment of Ramos cells with an isotype control ADC (Supplementary Fig. S3).

Following ADCT-602 binding, internalization, and trafficking to lysosomes, SG3249 was cleaved, releasing SG3199 inside the cells. DNA ICLs were measured using a modification of the single-cell gel electrophoresis (Comet) assay, and crosslinking was expressed as the percentage decrease in Olive tail moment versus control irradiated cells. After a 2-hour exposure of Ramos cells to ADCT-602, crosslink formation occurred (**Fig. 1B**). Immediately after the drug incubation period, a low level of ICLs (3%) was observed, which increased over time to near peak levels (∼50%) at 12 hours and persisted up to 48 hours. In contrast, SG3199 immediately induced a high level of ICLs (46%) after drug incubation, which further increased to 56% after 2 hours and persisted up to 48 hours. An equivalent concentration of the nonbinding control ADC produced DNA ICLs over 48 hours in the same pattern as ADCT-602 but at much lower levels (the peak was ∼18% at 12 hours). In the CD22-negative cell line (KARPAS-299), ADCT-602 produced a low level of DNA ICLs (∼15%) over 48 hours

Table 1. Mean CD22 molecules/cell in a panel of hematological tumor cell lines and mean IC_{50} values of ADCT-602, an isotype control ADC, and the PBD dimer cytotoxin SG3199.

	Daudi	NAMALWA	Ramos	DO HH-2	GRANTA-519	MEC-2	NALM-6	REH	SEM	KM-H2	SUP-T1	KARPAS-299
Tumor type	BL	BL	BL	FL	MCL	CLL	B-ALL	B-ALL	B-ALL	HL	T-LL	ALCL
CD22 receptor copy number ± SEM	122,938 ± 56,908	17,670 ± 221	43,005 ± 1,117	202,470 ± 15,718	19,207 ± 282	69,291 ± 2,670	14,825 ± 142	16,835 ± 99	24,704 ± 335	—[a]	—[a]	—[a]
SG3199 IC_{50}, nmol/L ± SEM	0.008 ± 0.001	0.014 ± 0.001	0.016 ± 0.001	0.007 ± 0.001	0.002 ± 0	0.033 ± 0.009	0.002 ± 0	0.001 ± 0	0.005 ± 0.002	0.036 ± 0.005	0.026 ± 0.005	0.025 ± 0.001
ADCT-602 IC_{50}, nmol/L ± SEM	0.07 ± 0.021	2.27 ± 0.052	0.06 ± 0.021	0.06 ± 0.009	0.02 ± 0.0005	0.18 ± 0.050	0.11 ± 0.018	0.05 ± 0.006	0.52 ± 0.080	11.4 ± 1.11	9.34 ± 1.02	51.7 ± 3.86
B12-C220-SG3249 IC_{50}, nmol/L ± SEM	1.6 ± 0.145	2.63 ± 0.154	2.21 ± 0.797	0.66 ± 0.038	0.11 ± 0.004	3.43 ± 0.665	0.50 ± 0.044	0.64 ± 0.054	1.65 ± 0.148	6.29 ± 0.184	6.98 ± 0.433	22.4 ± 2.43

Note: Data are presented as mean ± SEM, calculated from three independent experiments.
Abbreviations: ALCL, anaplastic large cell lymphoma; B-ALL, B-cell acute lymphoblastic leukemia; BL, Burkitt lymphoma; CLL, chronic lymphocytic leukemia; FL, follicular lymphoma; HL, Hodgkin lymphoma; IC_{50}, 50% inhibitory concentration; MCL, mantle cell lymphoma; T-LL, T-cell lymphoblastic lymphoma.
[a]Data were below the limit of quantification for the assay.

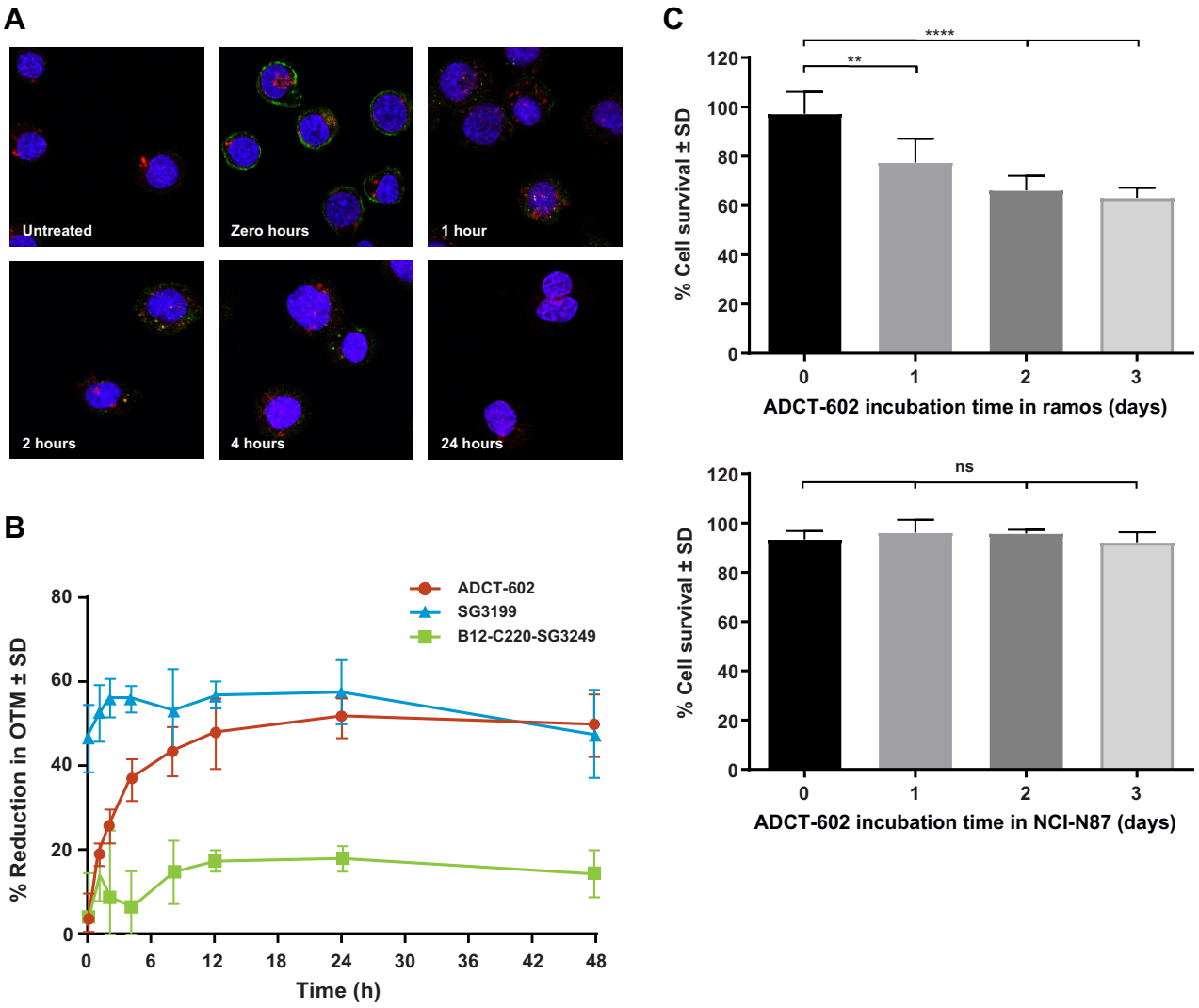

Figure 1.

Mode-of-action studies with ADCT-602. **A,** Confocal microscopy images of Ramos cells treated with 2 μg/mL ADCT-602 and stained for nuclei (blue), lysosomal-associated membrane protein 1 (LAMP-1; red), and human IgG antibody (green). **B,** Time course of DNA interstrand crosslink formation in Ramos cells exposed to ADCT-602 or free warhead SG3199. Percentage reduction in OTM relative to untreated control in Ramos cells treated with either 10 nmol/L ADCT-602 or 10 pmol/L SG3199. For ADCT-602, the peak of DNA crosslinking occurred at around 12 hours and persisted for 48 hours. **C,** Histograms depicting the percentage of viable CD22-negative KARPAS-299 cells after exposure to conditioned media from Ramos cells (top) or NCI-N87 cells (bottom) treated with ADCT-602 for different days (unpaired *t*-test). *, Co-staining between LAMP-1 and IgG is observed as yellow. Crosslinking and bystander data are presented as the mean of at least three independent experiments. **, $P < 0.05$; ****, $P < 0.0001$. IgG, immunoglobulin G; OTM, Olive tail moment.

following a 2-hour treatment (Supplementary Fig. S4). In this cell line, SG3199 produced a high level of ICL (~50%), similar to that observed in the Ramos cell line.

To determine whether ADCT-602 induces bystander killing of non–CD22-expressing cells, CD22-expressing Ramos cells were treated with ADCT-602 for 1, 2, or 3 days before transferring the conditioned media onto CD22-negative KARPAS-299 cells and incubating them for 96 hours. The ADCT-602–conditioned medium elicited a bystander effect after 1 day of pretreatment, as shown by a decrease in the percentage survival in the conditioned medium-treated KARPAS-299 cells, compared with the nonconditioned medium (97% to 78%, $P = 0.001$; **Fig. 1C**, top). The bystander effect increased after 2 to 3 days of preincubation in Ramos cells, as shown by a further decrease in the percentage of cell survival compared with the nonconditioned medium (66% and 62%, $P < 0.0001$). Conversely, when the conditioned medium from ADCT-602–treated, CD22-negative NCI-N87 cells was transferred to KARPAS-299, no significant change in the percentage of cell survival was measured compared with the nonconditioned medium (**Fig. 1C**, bottom).

ADCT-602 has strong *in vivo* antitumor activity in CD22-positive lymphoma and leukemia xenograft models

ADCT-602 demonstrated dose-dependent antitumor activity against both subcutaneous and disseminated tumor *in vivo* models. In the subcutaneous Ramos xenograft, a single dose of ADCT-602 at 0.3 and 1 mg/kg induced specific and dose-dependent antitumor

activity compared with the vehicle and the isotype control ADC. The 1 mg/kg ADCT-602 dose resulted in 10 of 10 complete responses and 9 of 10 tumor-free survivors at the end of the study (day 60; **Fig. 2A**). The resulting Kaplan–Meier survival curves showed the dose-dependent extension of survival (log-rank test, $P \leq 0.01$ for each comparison; Supplementary Fig. S5A).

In the subcutaneous WSU-DLCL2 xenograft model, a single dose of ADCT-602 at 1 and 3 mg/kg induced dose-dependent antitumor

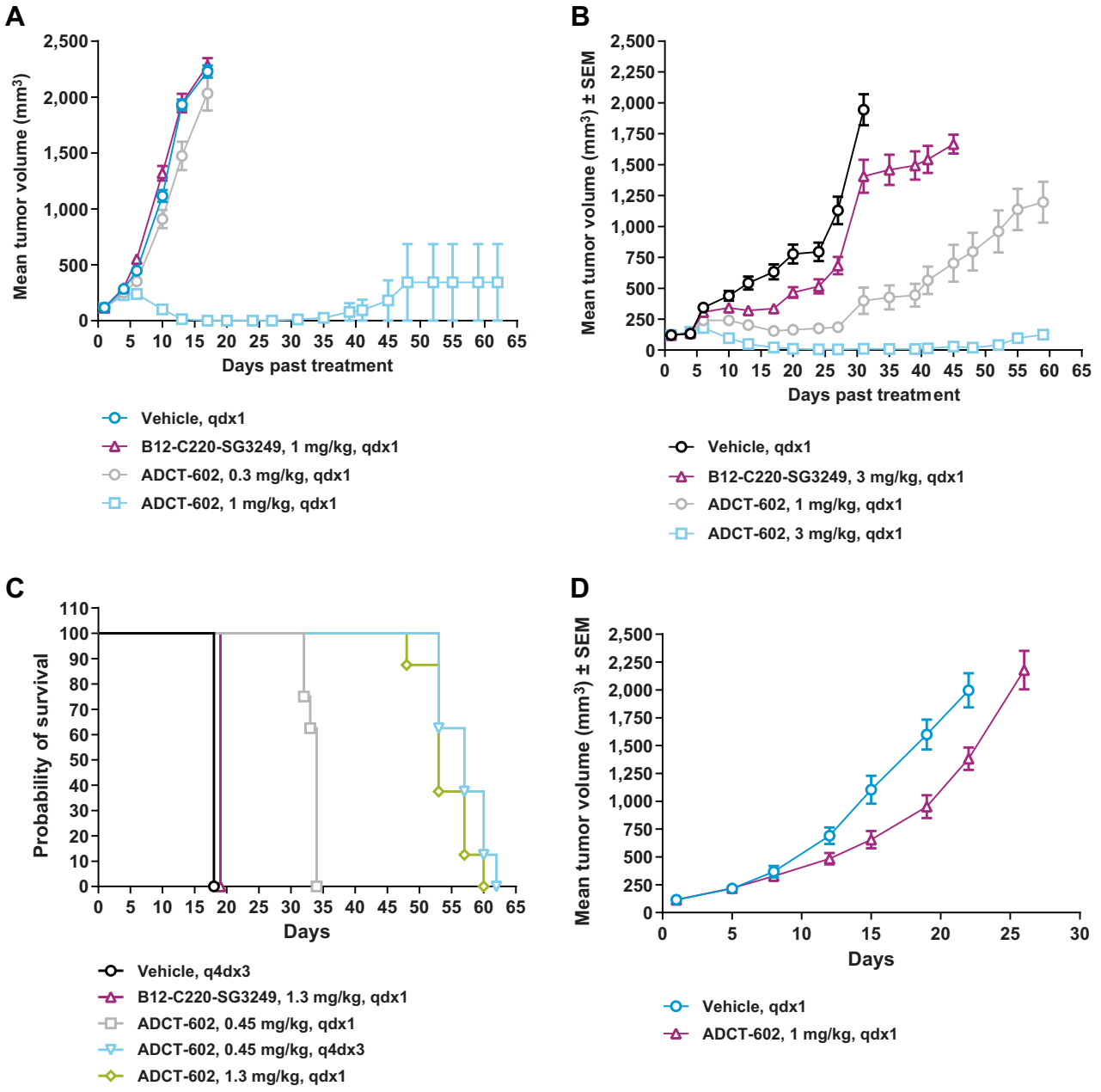

Figure 2.

In vivo antitumor activity of ADCT-602 in a range of xenograft models. **A,** *In vivo* antitumor activity of ADCT-602 in an subcutaneously implanted Burkitt lymphoma–derived Ramos xenograft model. ADCT-602 or an isotype-control ADC was administered intravenously at a group mean tumor volume of 116 mm^3 as a single dose to treatment groups of 10 mice. A vehicle-treated group served as the control. **B,** *In vivo* antitumor activity of ADCT-602 in an subcutaneously implanted DLBCL-derived WSU-DLCL2 xenograft model. ADCT-602 or an isotype-control ADC was administered intravenously at a group mean tumor volume of 121 mm^3 as a single dose to treatment groups of 10 mice. A vehicle-treated group served as the control. **C,** *In vivo* antitumor activity of ADCT-602 in a disseminated REH model. Kaplan–Meier survival plots show the percentage of animal survival over 62 days in an experiment in which ADCT-602 was administered either as a single dose of 0.45 mg/kg and 1.3 mg/kg or as multiple doses of 0.45 mg/kg Q4D × 3 and compared with the vehicle or nontargeting ADC administered as a single dose of 1.3 mg/kg (each group, $n = 8$). **D,** Lack of *in vivo* antitumor activity of ADCT-602 in CD22-negative KARPAS-299 ALCL xenograft. ADCT-602 was administered intravenously (day 1) to treatment groups of 8 mice. A vehicle-treated group served as the control. ADC, antibody–drug conjugate; ALCL, anaplastic large cell lymphoma; DLBCL, diffuse large B-cell lymphoma; QD, daily; Q4D, every 4 days; SC, subcutaneous(ly).

activity compared with the vehicle and the isotype control ADC. The 3 mg/kg ADCT-602 dose resulted in 3 of 10 partial responders, 7 of 10 complete responses, and 2 of 10 tumor-free survivors at the end of the study (day 59; **Fig. 2B**). The resulting Kaplan–Meier survival curves showed the dose-dependent extension of survival (log-rank test, $P \leq 0.05$ for each comparison; Supplementary Fig. S5B).

In a disseminated B-ALL–derived xenograft model (REH), a single dose of ADCT-602 at 0.45 mg/kg and 1.3 mg/kg resulted in a dose-dependent extension of survival compared with the vehicle and the isotype control ADC (log-rank test, $P \leq 0.001$; **Fig. 2C**). A single 1.3-mg/kg dose of ADCT-602 resulted in a comparable survival time to the equivalent fractionated dose of ADCT-602 [0.45 mg/kg, every 4 days, for three times (Q4D × 3)].

Finally, in the subcutaneous KARPAS-299 xenograft model (a CD22-negative T-cell lymphoma–derived model), a single 1-mg/kg dose of ADCT-602 had no significant antitumor activity compared with the vehicle group at the end of the study (day 29; **Fig. 2D**).

In all models, treatments were well tolerated, and no clinical observations were reported. Although body weight loss is always observed in the final stage of leukemia development in mice due to the infiltration of leukemic cells into all organs, body weight loss was minimal (Supplementary Fig. S6).

Toxicology and pharmacokinetic studies with ADCT-602

The toxicity of ADCT-602 was evaluated in rats and cynomolgus monkeys. Of these species, only the cynomolgus monkey is pharmacologically relevant, with the antibody component of ADCT-602 binding to human and cynomolgus monkey CD22 but not rat CD22. In the toxicity study in Sprague-Dawley rats, animals received a single intravenous bolus dose of 2 mg/kg ADCT-602 and survived until the scheduled termination on day 21. Administration of ADCT-602 was associated with a reduction in body weight gain (−47% by the end of the study) and with changes in hematology parameters [including reductions in white blood cell (−61%), platelet (−72%), reticulocyte (−43%), and lymphocyte counts (−54%)] on day 8 that reversed completely by day 21. The exposure profiles determined using a total antibody, a CD22 antigen capture, and an ADC-specific assay (detecting conjugate species with a DAR ≥1) were similar, with the curves determined using the total Ab and CD22 capture assay completely overlapping (**Fig. 3A**), indicating that ADCT-602 is stable *in vivo*. Toxicokinetic analysis indicated a half-life of approximately 8 days for ADCT-602 in rats (Supplementary Table S5). In the toxicity study in cynomolgus monkeys, animals received 0.6 or 0.9 mg/kg ADCT-602 on days 1 and 22 by 30-minute intravenous infusion. While the 0.6 mg/kg dose of ADCT-602 was tolerated, with all animals surviving until scheduled termination on day 43, animals at the 0.9 mg/kg dose were terminated prematurely on days 30 and 31 due to adverse clinical signs, including a hunched posture and >15% body weight loss in 2 of 3 animals (Supplementary Fig. S7). At both dose levels, CD20$^+$ B cells were completely depleted from circulation by day 15, consistent with the mode of action of ADCT-602; at 0.6 mg/kg, CD20$^+$ B cells remained depleted until day 43 (**Fig. 3B**). Other white blood cell parameters were largely unaffected by administration of ADCT-602 (Supplementary Fig. S8). The exposure profiles upon administration of ADCT-602, determined using a total antibody and ADC-specific (DAR ≥1) assay, were comparable, indicating *in vivo* stability of ADCT-602. Transient, low levels of free SG3199 warhead were only detectable shortly after dosing (≤ 0.3 ng/mL). Toxicokinetic analysis indicated a half-life of 4–5 days for ADCT-602 in cynomolgus monkeys (**Fig. 3C**; Supplementary Table S5). At necropsy, ADCT-602-related findings in histopathology evaluations were noted in the bone marrow, thymus, spleen, Peyer's patches, mandibular and mesenteric lymph nodes, testes, and kidneys. Findings in the spleen, Peyer's patches, and lymph nodes were considered to be at least partially related to the mechanism of action of ADCT-602 (i.e., CD22$^+$ cell depletion) and consisted of lymphoid depletion and decreased cellularity or a complete loss of germinal centers. In the kidneys of all animals and in the testes of 1 sexually mature male, tubulointerstitial nephropathy and tubular atrophy, characterized by loss of all spermatocyte stages, were noted, respectively, consistent with findings observed in other ADCs with the SG3249 payload. Finally, in the bone marrow of the animals dosed at 0.9 mg/kg, minimal-to-marked decreased cellularity was noted as a consequence of depletion of hematopoietic cells of all lineages. On the basis of these findings, the highest nonseverely toxic dose (HNSTD) for ADCT-602 in this study was considered to be the 0.6 mg/kg dose, similar to the HNSTD of loncastuximab tesirine [loncastuximab tesirine-lpyl (Lonca); ZYNLONTA] in a study of similar design.

Gene expression signature association analysis and combination studies with ADCT-602

A gene expression signature association analysis was performed on the 48 B-cell lymphoma cell lines tested with ADCT-602 (Supplementary Table S1; Supplementary Table S3) to search for pathways associated with resistance (median IC_{50} value >200 pmol/L; $n = 25$) or sensitivity (median IC_{50} value <200 pmol/L; $n = 23$) to ADCT-602. A total of 1,207 genes were identified as downregulated (logFC-negative) and 1,104 genes as upregulated (logFC-positive) in the resistant cell lines (Supplementary File S1). To delineate the pathways associated with the different degrees of sensitivity to ADCT-602, a gene-set enrichment analysis was performed on the preranked *limma* data. Transcripts upregulated in the resistant cell lines were enriched for genes coding proteins involved in respiratory electron transport, oxidative phosphorylation, and proteasome (**Fig. 4A**; Supplementary Data S1). Conversely, transcripts upregulated in cell lines sensitive to ADCT-602 were enriched for genes coding proteins involved in inflammation, p53 response, IL2/STAT5 signaling, hypoxia, and TGFβ and IFN response (**Fig. 4B**; Supplementary File S1). Because *IRAK1* was among the differentially expressed genes associated with resistance to ADCT-602, we hypothesized that sensitivity to ADCT-602 could be restored by combining ADCT-602 with pacritinib (a selective Janus kinase 2, FMS-like tyrosine kinase 3, and *IRAK1* multikinase inhibitor; ref. 31). In cell lines with low *IRAK1* expression that were sensitive to ADCT-602, the combination was additive in 2 of 4 cell lines, while no benefit was observed in the other 2 of 4 cell lines (**Fig. 5A**). In cell lines with high *IRAK1* expression that were resistant to ADCT-602, the combination was synergistic in 2 of 4 cell lines, was additive in 1 of 4, and had no beneficial effect in the remaining cell line. In MCL cells, the combination was not beneficial in cell lines with low *IRAK1* expression that were sensitive to ADCT-602, but the combination reached synergism in cell lines with high *IRAK1* expression that were resistant to ADCT-602.

It has been suggested that chidamide, a histone deacetylase inhibitor, promotes the expression of CD22 on the surface of B-cell tumor cells and enhances the function of CD22 in chimeric antigen receptor T-cell therapy (32). Therefore, we tested whether pretreatment of lymphoma cell lines with chidamide could enhance ADCT-602 activity by increasing CD22 expression. Pretreatment with chidamide increased CD22 expression up to 2.4 times compared with DMSO-pretreated cells (**Fig. 5B**), and ADCT-602 IC_{50} improved up to 2.5 times compared with DMSO-pretreated cells (**Fig. 5C**). Conversely, no effect on the cytotoxicity of the

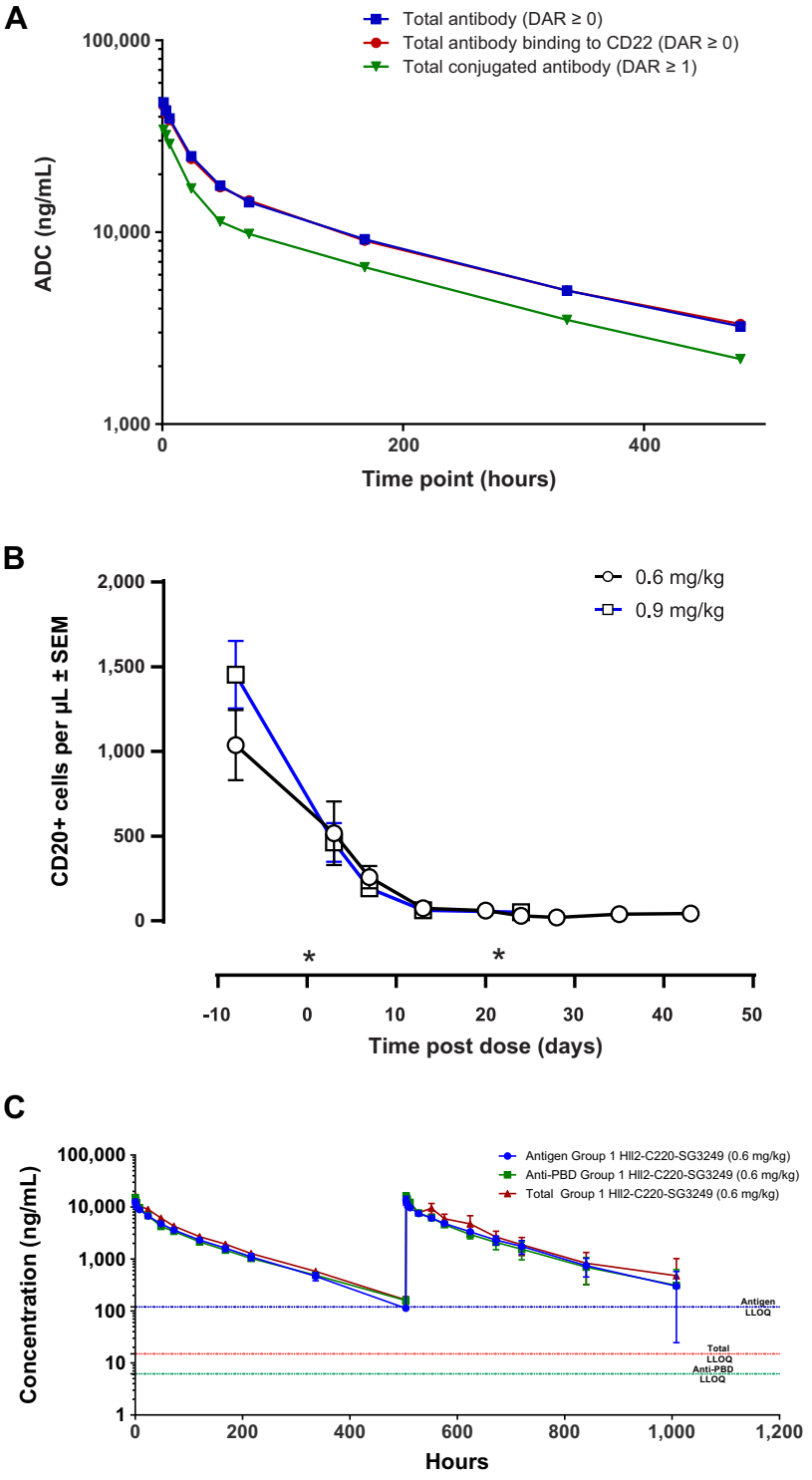

Figure 3.

Pharmacokinetics and pharmacodynamics in rats and cynomolgus monkies. **A,** Pharmacokinetics of ADCT-602 in rats (three in total) as measured by total antibody ECLIA, ADC (DAR ≥1) ECLIA, or total extracellular CD22-binding antibody ECLIA. **B,** B-cell depletion after dosing ADCT-602 in cynomolgus monkies (three in total). **C,** Pharmacokinetics of ADCT-602 in cynomolgus monkies as measured by the total antibody ECLIA, ADC (DAR ≥1) ECLIA, or total extracellular CD22-binding antibody ECLIA. *Indicates time of dosing. ADC, antibody–drug conjugate; DAR, drug-to-antibody ratio; ECLIA, electrochemiluminescence immunoassay; LLOQ, lower limit of quantification.

isotype-control ADC was seen across the three cell lines treated with chidamide (Supplementary Fig. S9).

Discussion

Here we report preclinical data for ADCT-602, a novel site-specific, PBD dimer–based, CD22-targeting ADC. ADCT-602 is based on reversed cysteine engineering of the IgG1 hinge, forcing conjugation on 1 cysteine of the heavy chain. The advantage of this format is that it provides a maximal DAR of 2, with no need for purification to remove any undesired higher DAR species.

The cytotoxic payload tesirine, which uses SG3199, is used in Lonca, which is approved by the FDA for use in R/R DLBCL based on strong single-agent activity in this hard-to-treat patient population, and in

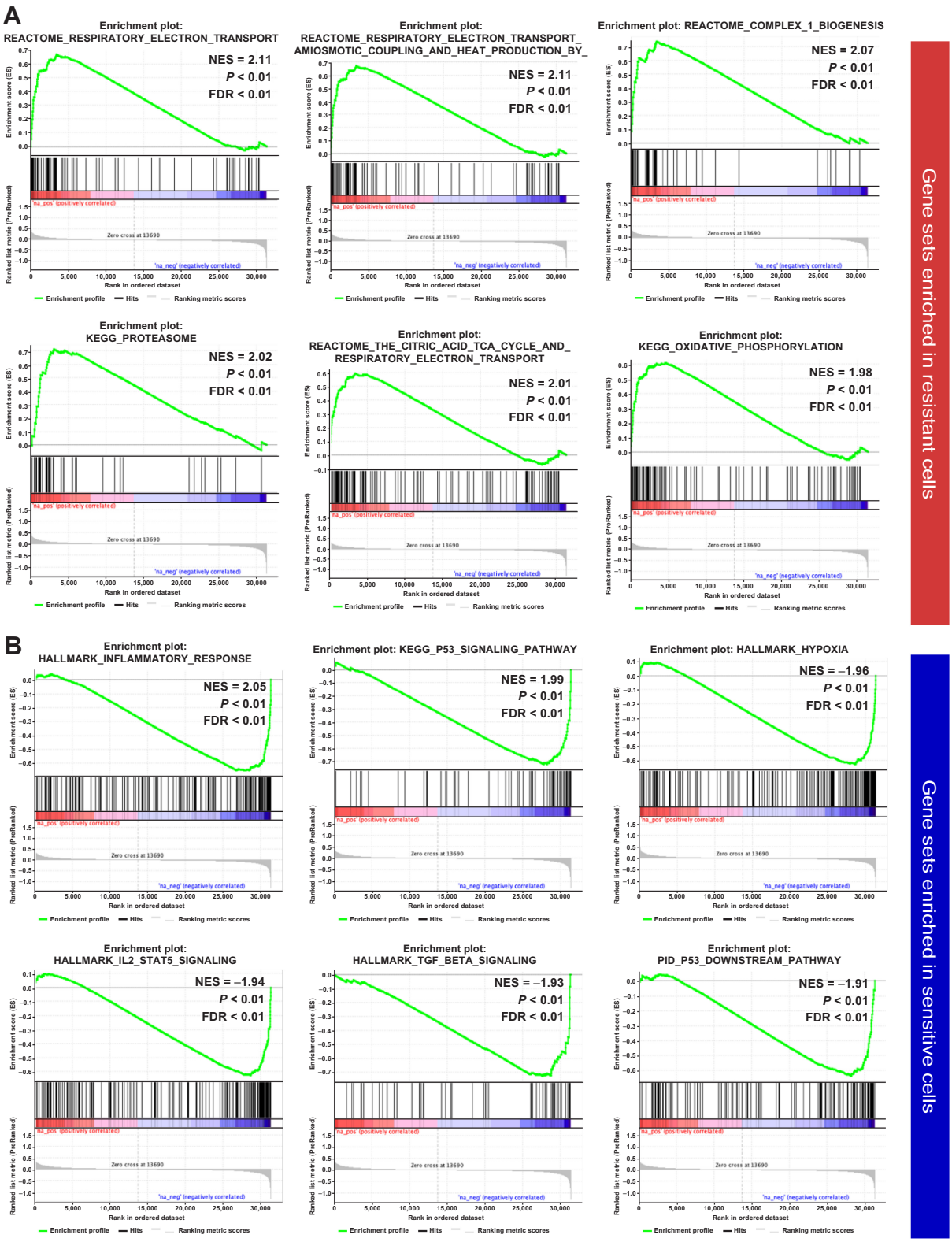

Figure 4.

Gene expression signature association analysis. Representative gene set enrichment analysis plots associated with resistance (**A**) to ADCT-602 [gene sets with higher expression in resistant cells (red)] and sensitivity (**B**) to ADCT-602 [gene sets with higher expression in sensitive cells (blue)] in B-cell lymphomas. NES, normalized enrichment score.

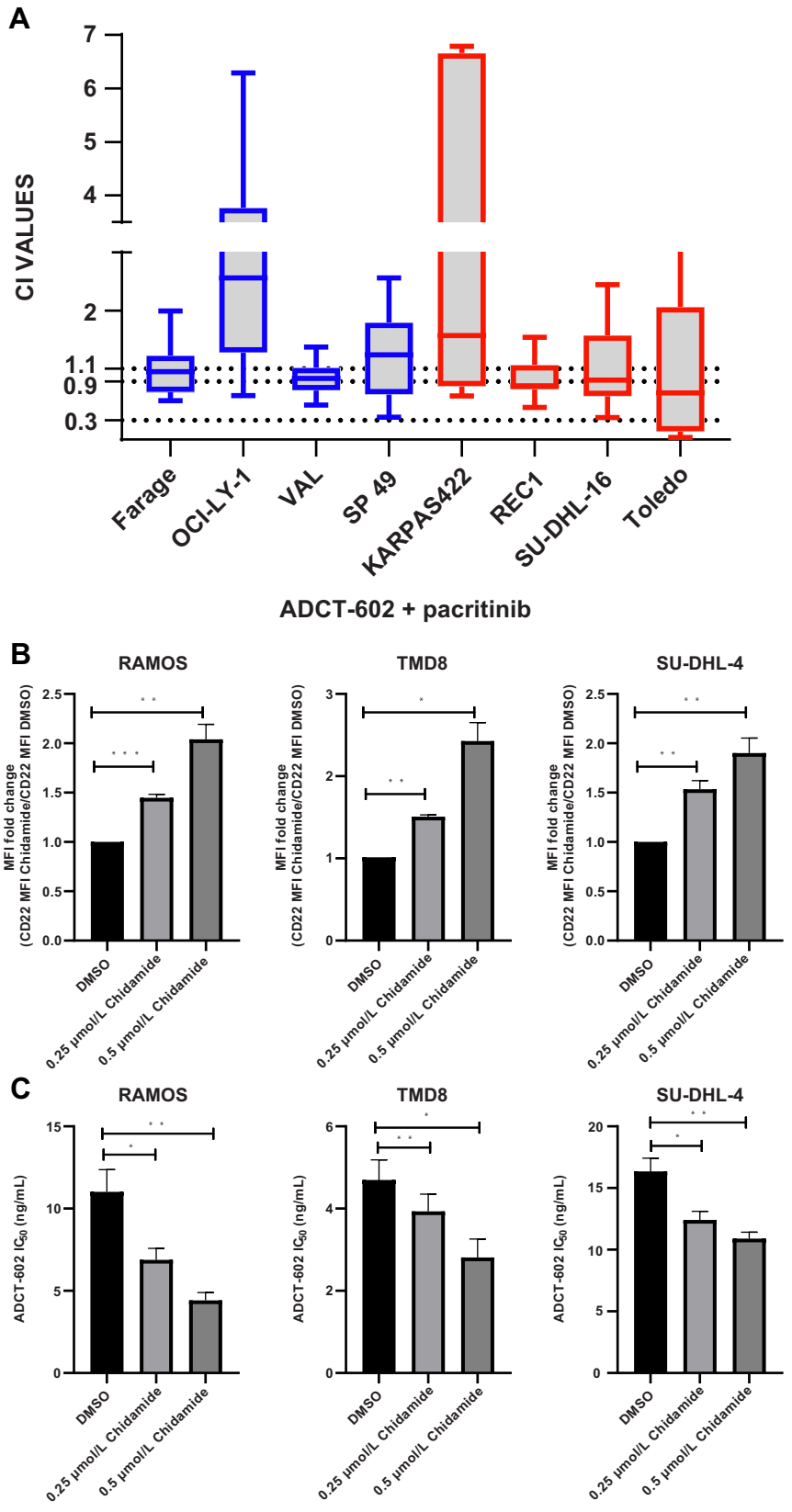

Figure 5.

Combination studies with ADCT-602. **A,** Box plots of the combination of ADCT-602 with pacritinib in eight lymphoma cell lines [four high *IRAK1* expression levels resistant to ADCT-602 (red; KARPAS-422, REC1, SU-DHL-16, and TOLEDO) and four low *IRAK1* expression levels sensitive to ADCT-602 (blue; FARAGE, OCI-LY-1, VAL, and SP49)]. Box plots represent the CI values obtained in individual cell lines. In each box plot, the line in the middle represents the median, and the box extends from the 25th to the 75th percentile; the whiskers extend to the upper and lower adjacent values. On the basis of the Chou–Talalay CI, the effect of the combinations was defined as synergistic (CI <0.9), additive (CI, 0.9–1.1), or antagonist (CI >1.1). CI thresholds are visualized with dotted lines. **B,** Cell-surface expression of CD22 following treatment with chidamide analyzed by flow cytometry in Ramos, TMD8, and SU-DHL-4 cell lines. Data represent the mean ± SE of at least two independent experiments, and they are expressed as MFI fold change (CD22 MFI chidamide/CD22 MFI DMSO). **C,** *In vitro* cytotoxicity of ADCT-602 following pretreatment with chidamide for 7 days. Data are presented as the mean IC_{50} values of ADCT-602 from at least three independent experiments. Statistics were calculated using an unpaired *t* test. CI, combination index; DMSO, dimethyl sulfoxide; IC_{50}, 50% inhibitory concentration; MFI, mean fluorescence intensity.

camidanlumab tesirine, which has encouraging phase II data in patients with R/R Hodgkin lymphoma (33, 34). Previous attempts to develop CD19-based ADCs in R/R DLBCL using other toxins had limited success, indicating that the PBD dimer toxin differentiates favorably in these patients. This favorable differentiation is also reflected in the safety profile. For example, inotuzumab ozogamicin and gemtuzumab ozogamicin, which use calicheamicin, have been linked to veno-occlusive disease, which is unlikely to occur with ADCT-602, based on the extensive clinical experience with Lonca and camidanlumab tesirine.

ADCT-602 showed potent *in vitro* activity in B-ALL and in a large panel of B-cell lymphoma subtypes, such as DLBCL and MCL, but not in T-cell non-Hodgkin lymphoma, which is in line with the absence of CD22 on these cells. This indicates CD22 expression is required for the activity of ADCT-602, although no correlation was found between ADCT-602 cytotoxicity and the CD22 receptor copy number. This is similar to what was described for the CD22-specific, auristatin-based ADC, pinatuzumab vedotin (DCDT2980S; refs. 4, 20, 35). Evidence of rapid internalization of ADCT-602 was provided by the reduction in the intensity of membrane immunofluorescence staining on CD22-expressing Ramos cells and LAMP-1 colocalization studies, suggesting that the processing of ADCT-602 is, at least in part, lysosomal. Similar to what was shown for Lonca (27), the time lag observed between the peaks of DNA ICL formation by ADCT-602 and by SG3199 reflects the time taken for internalization and cellular processing of the ADC compared with the readily diffusible PBD dimer SG3199. The crosslinks were persistent and detected over the observation period of 48 hours. ADCT-602 and Lonca both exhibited bystander toxicity of target-negative tumor cells. In medium transfer experiments, CD22-negative KARPAS-299 cells were killed by a soluble factor released from ADCT-602–treated Ramos cells into the medium. This soluble factor is assumed to be SG3199, released by lysosomal cleavage of ADCT-602 in the CD22-positive Ramos cells.

In vivo, ADCT-602 was remarkably effective against lymphoma and leukemia xenograft models in both subcutaneous and disseminated settings. A single ADCT-602 dose selectively delivered sufficient cytotoxic agent not only to delay tumor growth but also to achieve sustained tumor regression and, in many cases, tumor eradication. Interestingly, in the disseminated REH model, a single 1.35 mg/kg ADCT-602 dose was equally active as a fractionated ADCT-602 dose (0.45 mg/kg Q4D×3). Overall, the *in vivo* activity of ADCT-602 was similar to that of Lonca (27). In addition, B-cell depletion studies in cynomolgus monkeys showed that ADCT-602 was pharmacologically active (complete and sustained B-cell depletion) and well tolerated at 0.6 mg/kg with a half-life of ∼4.5 days. The pharmacokinetic profile confirmed the excellent stability of the C220 conjugation site in cynomolgus monkeys, with similar *in vivo* stability observed in the rat model.

An exploratory analysis comparing the expression profile of sensitive and resistant models identified *IRAK1* as 1 of the differentially expressed genes associated with ADCT-602 resistance in lymphoma cell lines. The combination with pacritinib was evaluated in eight lymphoma cell lines, four with high *IRAK1* expression levels that were resistant to ADCT-602 and four with low *IRAK1* expression levels that were sensitive to ADCT-602. The combination of ADCT-602 with pacritinib was more beneficial in cell lines with high *IRAK1* expression levels that were resistant to ADCT-602 compared with cell lines with low *IRAK1* expression levels that were sensitive to ADCT-602. These data suggest *IRAK1* is a potential marker of ADCT-602 resistance. In addition, treatment of B-cell lymphoma cell lines with the histone deacetylase inhibitor chidamide produced an increased expression of membranous CD22, which resulted in increased but specific ADCT-602 cytotoxicity, suggesting histone deacetylase inhibitors may potentially be combination partners for ADCT-602. Further confirmation of these findings in *in vivo* studies is currently being planned.

Altogether, these impressive preclinical data support the rapid clinical testing of ADCT-602 in patients with CD22-expressing B-cell malignancies. ADCT-602 is currently being evaluated in a phase I clinical study (NCT03698552), which reported promising early signs of clinical activity in heavily pretreated patients with B-ALL, warranting further investigation (36, 37). In addition, because ADCT-602 targets CD22 rather than CD19, it has the potential to be sequenced before or after other approved treatment modalities for B-cell malignancies that target CD19 (38).

Authors' Disclosures

F. Zammarchi reports a patent for Combination ADCT-602 with other drugs pending. K.E. Havenith reports other support from ADC Therapeutics outside the submitted work. C. Tarantelli reports Travel grant from iOnctura. F. Bertoni reports other support from ADC Therapeutics and grants and other support from HTG Molecular Diagnostics during the conduct of the study; grants from BeiGene; other support from Bayer AG, Helsinn, Ideogen AG, Ideogen AG, Idorsia Pharmaceuticals Ltd, Immagene, ImmunoGen, Menarini Ricerche, Nordic Nanovector ASA, Onctternal Therapeutics, Spexis AG, BIMINI Biotech, Novartis, Amgen, Astra Zeneca, and other support from iOnctura outside the submitted work; in addition, F. Bertoni has a patent for Combination Therapy pending. J.A. Hartley reports grants from ADC Therapeutics during the conduct of the study. P.H. van Berkel reports a patent for US10722594B2 issued to ADC Therapeutics SA. No disclosures were reported by the other authors.

Authors' Contributions

F. Zammarchi: Design of experiments, data interpretation, figure preparation, manuscript writing. **K.E. Havenith:** Design of experiments, data interpretation. **N. Sachini:** Design and performance of experiments. **N. Janghra:** Design and performance of experiments. **S. Chivers:** Design of experiments, data interpretation. **E. Idusogie:** Design of experiments, data interpretation. **E. Gaudio:** Design and performance of experiments. **C. Tarantelli:** Design and performance of experiments. **F. Bertelli:** Design of experiments, data interpretation. **K. Santos:** Design and performance of experiments. **P. Tyrer:** Design and performance of experiments. **S. Corbett:** Design and performance of experiments. **F. Spriano:** Design and performance of experiments. **G. Golino:** Design and performance of experiments. **L. Cascione:** Design and performance of experiments. **F. Bertoni:** Design of experiments, data interpretation. **J.A. Hartley:** Design of experiments, data interpretation. **P.H. van Berkel:** Data interpretation, guidance, and manuscript writing.

Acknowledgments

The authors thank Sterling for manufacturing the ADC. Charles River Laboratory Services, Epo-GmbH, and Covance (now Labcorp Drug Development) are thanked for conducting the *in vivo* studies. Medical writing and editorial support were provided by Claire Line, PhD, on behalf of Citrus Health Group, which was in accordance with Good Publication Practice (GPP 2022) guidelines and funded by ADC Therapeutics SA.

The publication costs of this article were defrayed in part by the payment of publication fees. Therefore, and solely to indicate this fact, this article is hereby marked "advertisement" in accordance with 18 USC section 1734.

Note

Supplementary data for this article are available at Molecular Cancer Therapeutics Online (http://mct.aacrjournals.org/).

Received August 4, 2023; revised November 22, 2023; accepted January 16, 2024; published first February 7, 2024.

References

1. Shah NN, Sokol L. Targeting CD22 for the treatment of B-cell malignancies. Immunotargets Ther 2021;10:225–36.
2. Nitschke L. CD22 and Siglec-G: B-cell inhibitory receptors with distinct functions. Immunol Rev 2009;230:128–43.
3. Hoelzer D. CD22 monoclonal antibody therapies in relapsed/refractory acute lymphoblastic leukemia. Cancer 2013;119:2671–4.
4. Li D, Poon KA, Yu SF, Dere R, Go M, Lau J, et al. DCDT2980S, an anti-CD22-monomethyl auristatin E antibody-drug conjugate, is a potential treatment for non-Hodgkin lymphoma. Mol Cancer Ther 2013;12:1255–65.
5. Polson AG, Williams M, Gray AM, Fuji RN, Poon KA, McBride J, et al. Anti-CD22-MCC-DM1: an antibody-drug conjugate with a stable linker for the treatment of non-Hodgkin's lymphoma. Leukemia 2010;24:1566–73.
6. Haso W, Lee DW, Shah NN, Stetler-Stevenson M, Yuan CM, Pastan IH, et al. Anti-CD22-chimeric antigen receptors targeting B-cell precursor acute lymphoblastic leukemia. Blood 2013;121:1165–74.
7. Piccaluga PP, Arpinati M, Candoni A, Laterza C, Paolini S, Gazzola A, et al. Surface antigens analysis reveals significant expression of candidate targets for immunotherapy in adult acute lymphoid leukemia. Leuk Lymphoma 2011;52:325–7.
8. Raponi S, De Propris MS, Intoppa S, Milani ML, Vitale A, Elia L, et al. Flow cytometric study of potential target antigens (CD19, CD20, CD22, CD33) for antibody-based immunotherapy in acute lymphoblastic leukemia: analysis of 552 cases. Leuk Lymphoma 2011;52:1098–107.
9. Leonard JP, Goldenberg DM. Preclinical and clinical evaluation of epratuzumab (anti-CD22 IgG) in B-cell malignancies. Oncogene 2007;26:3704–13.
10. Lindén O, Hindorf C, Cavallin-Ståhl E, Wegener WA, Goldenberg DM, Horne H, et al. Dose-fractionated radioimmunotherapy in non-Hodgkin's lymphoma using DOTA-conjugated, 90Y-radiolabeled, humanized anti-CD22 monoclonal antibody, epratuzumab. Clin Cancer Res 2005;11:5215–22.
11. Vose JM, Colcher D, Gobar L, Bierman PJ, Augustine S, Tempero M, et al. Phase I/II trial of multiple dose 131Iodine-MAb LL2 (CD22) in patients with recurrent non-Hodgkin's lymphoma. Leuk Lymphoma 2000;38:91–101.
12. Bhatta P, Whale KD, Sawtell AK, Thompson CL, Rapecki SE, Cook DA, et al. Bispecific antibody target pair discovery by high-throughput phenotypic screening using in vitro combinatorial Fab libraries. MAbs 2021;13:1859049.
13. NIH. A study of JNJ-75348780 in participants with non-Hodgkin lymphoma (NHL) and chronic lymphocytic leukemia (CLL). NCT04540796. Available from: https://www.clinicaltrials.gov/ct2/show/NCT04540796.
14. Shah NN, Stetler-Stevenson M, Yuan CM, Shalabi H, Yates B, Delbrook C, et al. Minimal residual disease negative complete remissions following anti-CD22 chimeric antigen receptor (CAR) in children and young adults with relapsed/refractory acute lymphoblastic leukemia (ALL). Blood 2016;128:650.
15. Tan Y, Cai H, Li C, Deng B, Song W, Ling Z, et al. A novel full-human CD22-CAR T cell therapy with potent activity against $CD22^{low}$ B-ALL. Blood Cancer J 2021;11:71.
16. Ingle GS, Scales SJ. DropArray™, a wall-less 96-well plate for uptake and immunofluorescence microscopy, confirms CD22 recycles. Traffic 2014;15:255.
17. Leung SO, Goldenberg DM, Dion AS, Pellegrini MC, Shevitz J, Shih LB, et al. Construction and characterization of a humanized, internalizing, B-cell (CD22)-specific, leukemia/lymphoma antibody, LL2. Mol Immunol 1995;32:1413–27.
18. Chu Y, Zhou X, Wang X. Antibody-drug conjugates for the treatment of lymphoma: clinical advances and latest progress. J Hematol Oncol 2021;14:88.
19. Tong JTW, Harris PWR, Brimble MA, Kavianinia I. An insight into FDA approved antibody-drug conjugates for cancer therapy. Molecules 2021;26:5847.
20. Morschhauser F, Flinn IW, Advani R, Sehn LH, Diefenbach C, Kolibaba K, et al. Polatuzumab vedotin or pinatuzumab vedotin plus rituximab in patients with relapsed or refractory non-Hodgkin lymphoma: final results from a phase 2 randomised study (ROMULUS). Lancet Haematol 2019;6:e254–65.
21. Kantarjian HM, DeAngelo DJ, Stelljes M, Martinelli G, Liedtke M, Stock W, et al. Inotuzumab ozogamicin versus standard therapy for acute lymphoblastic leukemia. N Engl J Med 2016;375:740–53.
22. Wynne J, Wright D, Stock W. Inotuzumab: from preclinical development to success in B-cell acute lymphoblastic leukemia. Blood Adv 2019;3:96–104.
23. Giles FJ, Kantarjian HM, Kornblau SM, Thomas DA, Garcia-Manero G, Waddelow TA, et al. Mylotarg (gemtuzumab ozogamicin) therapy is associated with hepatic venoocclusive disease in patients who have not received stem cell transplantation. Cancer 2001;92:406–13.
24. National Research Council. Guide for the care and use of laboratory animals. 8th ed. Washington, DC: The National Academies Press; 2011.
25. Cho S, Zammarchi F, Williams DG, Havenith CEG, Monks NR, Tyrer P, et al. Antitumor activity of MEDI3726 (ADCT-401), a pyrrolobenzodiazepine antibody-drug conjugate targeting PSMA, in preclinical models of prostate cancer. Mol Cancer Ther 2018;17:2176.
26. Flynn MJ, Zammarchi F, Tyrer PC, Akarca AU, Janghra N, Britten CE, et al. ADCT-301, a pyrrolobenzodiazepine (PBD) dimer-containing antibody-drug conjugate (ADC) targeting CD25-expressing hematological malignancies. Mol Cancer Ther 2016;15:2709–21.
27. Zammarchi F, Corbett S, Adams L, Tyrer PC, Kiakos K, Janghra N, et al. ADCT-402, a PBD dimer-containing antibody drug conjugate targeting CD19-expressing malignancies. Blood 2018;131:1094–105.
28. Spanswick VJ, Hartley JM, Hartley JA. Measurement of DNA interstrand crosslinking in individual cells using the single cell gel electrophoresis (Comet) assay. Methods Mol Biol 2010;613:267–82.
29. Tarantelli C, Gaudio E, Arribas AJ, Kwee I, Hillmann P, Rinaldi A, et al. PQR309 is a novel dual PI3K/mTOR inhibitor with preclinical antitumor activity in lymphomas as a single agent and in combination therapy. Clin Cancer Res 2018;24:120–9.
30. Ritchie ME, Phipson B, Wu D, Hu Y, Law CW, Shi W, et al. limma powers differential expression analyses for RNA-sequencing and microarray studies. Nucleic Acids Res 2015;43:e47.
31. Singer JW, Al-Fayoumi S, Ma H, Komrokji RS, Mesa R, Verstovsek S. Comprehensive kinase profile of pacritinib, a nonmyelosuppressive Janus kinase 2 inhibitor. J Exp Pharmacol 2016;8:11–9.
32. Yang X, Yu Q, Xu H, Zhou J. Upregulation of CD22 by chidamide promotes CAR T cells functionality. Sci Rep 2021;11:20637.
33. Caimi PF, Ai W, Alderuccio JP, Ardeshna KM, Hamadani M, Hess B, et al. Loncastuximab tesirine in relapsed or refractory diffuse large B-cell lymphoma (LOTIS-2): a multicentre, open-label, single-arm, phase 2 trial. Lancet Oncol 2021;22:790–800.
34. Carlo-Stella C, Ansell S, Zinzani PL, Radford J, Maddocks K, Pinto A, et al. Camidanlumab tesirine: updated efficacy and safety in an open-label, multicenter, phase 2 study of patients with relapsed or refractory classical Hodgkin lymphoma (R/R cHL). In: 27th Congress of the European Hematology Association; 2022 Jun 9–12; Vienna, Austria. Hague, the Netherlands: ESH; 2022. Abstract nr S201.
35. Advani RH, Lebovic D, Chen A, Brunvand M, Goy A, Chang JE, et al. Phase I study of the anti-CD22 antibody-drug conjugate pinatuzumab vedotin with/without rituximab in patients with relapsed/refractory B-cell non-Hodgkin lymphoma. Clin Cancer Res 2017;23:1167–76.
36. Jain N, Jabbour EJ, Aldoss I, Konopleva M, Short N, Stein AS, et al. ADCT-602, a CD22 targeting antibody drug conjugate bound to PBD toxin in adult patients with relapsed or refractory B-cell acute lymphoblastic leukemia: a phase 1 trial. Blood 2022;14 (Suppl 1):521–2.
37. Jain N, Jabbour EJ, Konopleva M, Pemmaraju N, Thompson PA, Short NJ, et al. A phase 1 trial of ADCT-602, a CD22 targeting antibody drug conjugate bound to PBD toxin in adult patients with relapsed or refractory CD22+ B-cell acute lymphoblastic leukemia. Blood 2021;138 (Suppl 1):1237.
38. Strüßmann T, Wäsch R, Scherer F, Mutter JA, Pfeifer D, Bartsch I, et al. A patient with refractory high-grade B-cell lymphoma and rapid progression under CAR-T-cell therapy was successfully salvaged with inotuzumab-ozogamicin. Leuk Lymphoma 2022;63:2260–2.